Nanoscale

Accepted Manuscript

This article can be cited before page numbers have been issued, to do this please use: Y. Zhang, K. Zhan, P. Xin, Y. Zhao, I. Alam, S. Wang, A. Hubarevich, K. Liu, X. Zhang and J. Huang, *Nanoscale*, 2026, DOI: 10.1039/D5NR04125B.

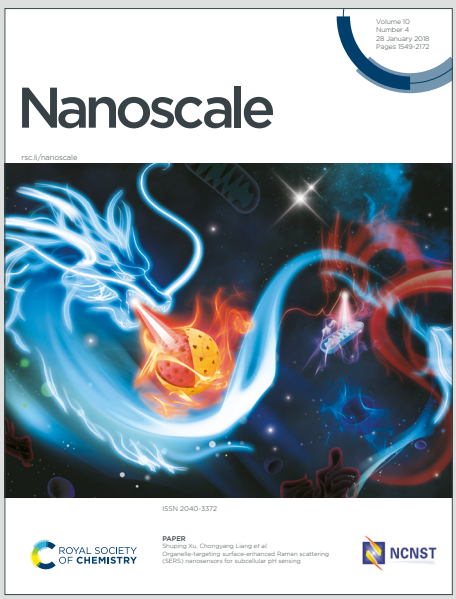

ROYAL SOCIETY OF CHEMISTRY

rsc.li/nanoscale

Nitrilotriacetic acid functionalized gold nanopillars enable stochastic detection and deep learning analysis of prolines and hydroxyprolines by surface enhanced Raman spectroscopy

Yuan Zhang [a], Kuo Zhan [a,b], Peilin Xin [a,b], Yingqi Zhao [a,b], Ibrar Alam [a], Shubo Wang [d], Aliaksandr Hubarevich [e], Kai Liu [f], Xuejin Zhang [f], Jianan Huang [a,b,c,*]

[a] *Research Unit of Health Sciences and Technology (HST), Faculty of Medicine, University of Oulu, Oulu 90220, Finland.*

[b] *Biocenter Oulu, University of Oulu, Oulu 90220, Finland.*

[c] *Research Unit of Disease Networks, Faculty of Biochemistry and Molecular Medicine, University of Oulu, Oulu 90220, Finland.*

[d] *Nano and Molecular Systems Research Unit, Faculty of Science, University of Oulu, Oulu 90570, Finland.*

[e] *Plasmon Nanotechology Unit, Istituto Italiano di Tecnologia, Via Morego 30, 16163 Genova, Italy*

[f] *School of Physics and College of Engineering and Applied Sciences, Nanjing University, Nanjing 210093, China.*

* *Corresponding author. Email: jianan.huang@oulu.fi*

Abstract

Proline hydroxylation is crucial for monitoring diseases related to collagen metabolism, analyzing metabolic pathways, and evaluating therapeutic or nutritional outcomes. However, the small differences in the hydroxyl group between prolines (Pro) and hydroxyprolines (Hyp) are challenging for reliable label-free discrimination by surface-enhanced Raman scattering (SERS) based on silver and gold nanoparticles. Adsorption of Pro and Hyp on metal colloids took 72 and 48 hours, respectively, which led to occupation of the colloid surface by Hyp and thus overwhelming SERS signals of Hyp against those of Pro. Here, we developed a stochastic SERS method to detect the prolines and hydroxyprolines within 30 minutes by functionalizing gold nanopillars with nitrilotriacetic acid (NTA) and nickel ions (Ni^{2+}) to form the NTA-Ni structure for reversible and transient binding of the Pro/Hyp. By analyzing the SERS time series of the NTA-Ni-Pro/Hyp using the event occurrence frequency, we extracted their SERS feature for study of binding kinetics and quantification with the detection limits down to 0.20 nM for Pro and 0.23 nM for Hyp in mixture, respectively. To overcome the signal fluctuation, we developed a one-dimensional convolutional neural network model to identify NTA-Ni-Pro and NTA -Ni-Hyp with high accuracies of 86.9% and 89.6%, respectively. Our study demonstrated a new SERS strategy of hydroxylation detection by combining stochastic sensing and deep learning analysis. The excellent practicality of our method is

View Article Online
DOI: 10.1039/D5NR04125B

promising for binding and analyzing post translational modifications in biofluids for biomedical complex quantitative analysis and early diagnosis of diseases.

Keywords

Gold nanopillars

Surface-enhanced Raman spectroscopy

Proline hydroxylation

Deep learning analysis

Stochastic sensing

1. Introduction

Proline (Pro) is an important proteinogenic amino acid, which has an exceptional structure and is fundamental for many metabolic processes [1]. Hydroxyproline (Hyp) is a non-essential amino acid derived from Pro through an oxygen sensing post-translational modification regulated tumor cell metastasis [2–7]. The modification occurs by prolyl hydroxylases that add a single hydroxyl group (-OH) to replace the hydrogen of the Pro pyrrolidine ring. Hyp can subtly influence the protein structures, activities, and properties of protein-protein interactions in the cell and play a pivotal role in cancer development and disease progression [8]. Therefore, distinguishing Hyp from Pro is crucial to studying collagen structure, monitoring diseases related to collagen metabolism, analyzing metabolic pathways, and evaluating therapeutic or nutritional outcomes [9,10].

Current methods for the detection of Pro and Hyp have limitations. The isatin paper assays based on the reaction between isatin and proline to form pyrrole blue are simple but not sensitive [11]. Colorimetric techniques, such as ninhydrin reactions, are reliable but are influenced by reaction variability [12]. High-performance liquid chromatography (HPLC) provides detailed amino acid profiles but is costly and time intensive [13]. Mass spectrometry offers high sensitivity and detailed modifications but requires expertise and expensive equipment [14]. Alternatively, surface-enhanced Raman spectroscopy (SERS) is promising for the detection of Pro and Hyp, because it combines the molecular specificity of vibrational Raman spectroscopy with high sensitivity to provide rich fingerprint information of analytes.

However, the small differences in molecular structure (-OH group with 17.01 Da) between Hyp and Pro is challenging for reproducible SERS detection of Pro and Hyp, which required a long physical adsorption time of the analytes on metal colloids [15–17]. For example, J. J. Cárcamo et al. [15] prepared silver colloids at a controlled and fixed pH, allowing the analyte to be physically adsorbed on the colloid surface to obtain unique and reproducible SERS spectra. Accordingly, the required adsorption time for Pro and Hyp in the silver colloids for distinguishable and reproducible SERS spectra were 72 hours for Pro and 48 hours for Hyp. Similarly, our recent single-molecule SERS

View Article Online
DOI: 10.1039/D5NR04125B

sensor employed gold colloids to distinguish SERS spectra of Hyp and Pro, which needed 48-hour incubation time to absorb the Hyp or Pro on the gold nanoparticles [16]. These works implied that physical adsorption would be difficult for practical SERS detection of mixtures of Hyp and Pro in biofluid due to their long adsorption time.

To decrease the detection time, an effective receptor is explored to uniquely bind both analytes on plasmonic nanostructures. One such trial was functionalized silver colloids with a covalent organic frame with carboxylate groups (Ag@COF-COOH) to capture the Hyp based on the hydrogen-binding mechanism for SERS detection[18]. The detection time (10-15 minutes) was much shorter than that of analyte adsorption on colloids, which was then used in fast Hyp detection in inferior milk. However, the authors did not demonstrate SERS detection of Pro. Meanwhile, the Ag@COF-COOH binding probability is the same for both Hyp and Pro, which means that it could not distinguish Hyp from Pro. This example highlighted the challenge of unique binding of Pro and Hyp due to the small hydroxyl group between them and inspired us to design a new binding and analysis strategy for fast detection of Pro and Hyp.

In this study, we bound nitrilotriacetic acid (NTA) with nickel cations (Ni^{2+}) to form the NTA-Ni structure as the receptor on plasmonic gold nanopillars (AuNPs) for stochastic SERS detection of Pro and Hyp in liquid within 30 minutes as shown in **Figure 1a, b**. The gold nanopillar has a stable wide-range hot spot (**Figure 1c, d**) to cover the long molecule moieties for reproducible SERS detection [19,20]. The SERS time-series signals of the bound NTA-Ni-Pro and NTA-Ni-Hyp (**Figure 1e, f**) were then analyzed and distinguished with a deep learning model.

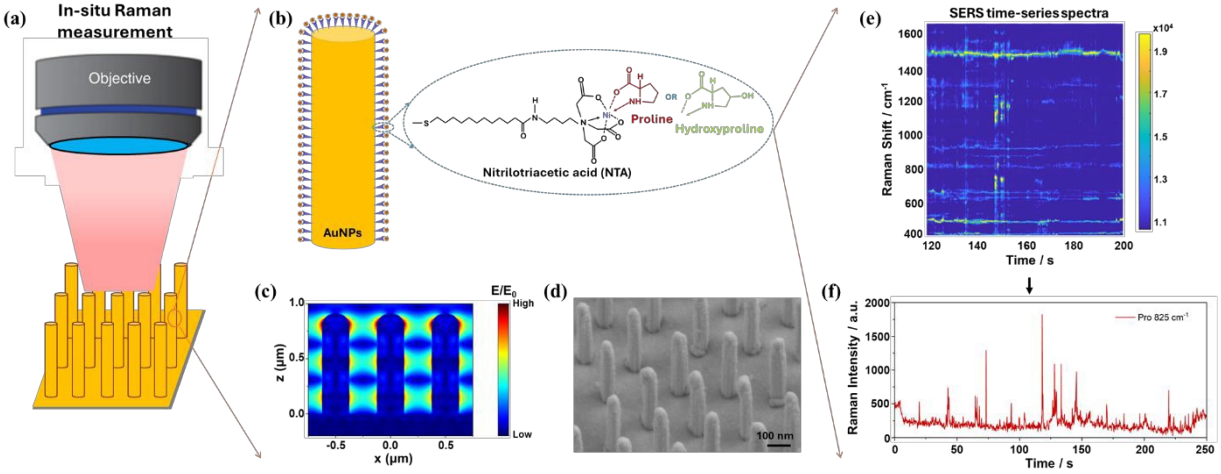

Figure 1. (a) In-situ Raman measurement of Pro and Hyp. (b) Schematic of the stochastic binding of Pro and Hyp using the NTA-Ni bond on the AuNPs. (c) Simulated electric field intensity distribution of AuNPs at 785 nm. The color bar shows the enhancement of the electric field intensity. (d) SEM image of AuNPs. (e) The time-series SERS spectra of AuNPs-NTA-Ni-Pro. The color bars show the intensities of SERS bands. (f) Corresponding SERS time trace after spectral processing of Pro.

Similar to that of the Histidine, the binding of Pro by the NTA-Ni was reversible and stochastic through chelation. Due to the five-membered ring structure in the side chain of Pro, NTA-Ni binding to Pro was found to be 10 times longer than it does to other proteogenic amino acids [21,22]. Because of the similar molecular structure of Hyp and Pro, the resultant SERS time-series of NTA-Ni-Pro and

View Article Online
DOI: 10.1039/D5NR04125B

NTA-Ni-Hyp would exhibit more Raman signals, or detection events, than those of other amino acids, which allow us to distinguish them by event frequency analysis [17]. Such method is significantly different from other SERS sensors based on NTA-metal complexes that detected the analytes by the intensity of SERS bands. For example, Li et al. fabricated gold nanoparticles substrates modified with NTA–Ni^{2+} complexes to capture histamine through the formation of NTA–Ni^{2+}–histamine coordination complexes [23]. The NTA–Ni^{2+}-decorated gold nanoparticles nanoprobe exhibited a detection sensitivity down to 1 μM for histamine. In another report, Kaya et al. employed AgNPs modified with NTA–Fe^{3+} complexes as SERS-active substrates for dopamine detection, even in the presence of ascorbic acid [24]. In this case, the formation of NTA–Fe^{3+}–dopamine complexes significantly amplified the Raman response, enabling detection at the picomolar (pM) level. Likewise, Cao et al. demonstrated sensitive SERS analysis of catecholamines using polyvinylpyrrolidone-capped AuNPs functionalized with NTA–Fe^{3+} complexes [25].

The SERS time series signals of NTA-Ni-Pro and NTA-Ni-Hyp were still similar, which will be analyzed for the binding kinetics and quantification based on the event frequencies of these biomolecules. Finally, combining the deep learning analysis using the convolutional neural network model, our method has identified the NTA-Ni-Pro and the NTA-Ni-Hyp with more than 90% accuracy with a detection limit of 0.1 pM. To the best of our knowledge, this is the first successful quantitative and fast analysis of Pro and Hyp using NTA as the receptor, which is promising for binding and analyzing post-translational modifications in biofluids for rapid biomedical analysis and early diagnosis of diseases.

2. Experimental section

Materials

Silicon wafers prime CZ-Si wafer 4-inch, thickness = 525 ± 25 μm, (111), 1-side polished, p-type (Boron), TTV < 10 μm, 1 - 10 Ohm cm was purchased from MicroChemicals GmbH; Polystyrene nanospheres of 0.5 μm diameter were purchased from Micro Particles GmbH; ethanol (CH_3CH_2OH) of purity ≥ 99.8%, AnalaR NORMAPUR® ACS, analytical reagent, nickel(II) chloride ($NiCl_2$) were purchased from Fisher Scientific; ethylene glycol ($HOCH_2CH_2OH$), acetone (CH_3COCH_3), sodium dodecyl sulfate solution (SDS, $CH_3(CH_2)_{11}OSO_3Na$), Hydrogen peroxide solution (H_2O_2), Hydrofluoric acid (HF), N-Nα,Nα-Bis(carboxymethyl)-L-lysine-12-mercaptododecanamide (NTA, $C_{22}H_{40}N_2O_7S$), L-Proline ($C_5H_9NO_2$), trans-4-Hydroxy-L-proline ($C_5H_9NO_3$), Cysteine ($C_3H_7NO_2S$), Histidine ($C_6H_9N_3O_2$), and Serine ($C_3H_7NO_3$) were purchase from Sigma-Aldrich.

Gold nanopillars fabrication

The fabrication of gold coated silicon pillars was based on the established nanosphere lithography protocol [19]. The procedures follow these steps, firstly, depositing 500 nm polystyrene nanospheres on the surface of 1x1 cm silicon wafers. The silicon wafers were hydrophilic by oxygen plasma (Gambetti Tecnologia colibri and bench-top plasma system, Italy), an automatic pump was

View Article Online
DOI: 10.1039/D5NR04125B

used to control the speed of polystyrene sphere droplet, and when polystyrene sphere occupied full of petri dish, the cleaned wafers were used to carry out the polystyrene sphere single layer. Allow the wafers with polystyrene sphere to be naturally dry, then reactive ion etching (RIE, Oxford Instruments Plasmalab 80 Plus PECVD/ICP-DRIE, UK) instrument was used to reduce the diameter of polystyrene nanospheres from 500 nm to 250 nm. After that, sputter coating (Quorumtech Q150T ES, UK) with 5 nm silver and 10 nm gold on the surface of silicon wafers. Then, ultrasonication for 5 minutes was performed to remove the polystyrene nanospheres. 20 mL of H_2O, 1 mL of HF and 0.2 mL of H_2O_2 solution were added one by one for chemical etching of the nanopillars. Finally, sputter coating 2 nm of titanium and 50 nm of gold for the nanopillars, then get the complete gold nanopillars chips. Electronic microscopic images of the nanopillars were taken by scanning electron microscopy (SEM, ZEISS Sigma HD VP FE-SEM, Germany). The reflectance of the as-made nanopillar chips was measured in the integrated sphere of ultraviolet–visible spectroscopy (UV-Vis, Shimadzu UV-2600, UK).

Sample preparation

Binding Ni^{2+} to NTA: 5 mL of 5 mM $NiCl_2$ was added to react with 5 mL of 5 mM NTA ethanol solution for 24 h to form an NTA-Ni structure.

Hydrophilicity of gold nanopillars: To clean the gold nanopillars, they were rinsed in ethanol and H_2O. Then, an oxygen plasma treatment (Gambetti Tecnologia colibri and bench-top plasma system, Italy) was performed to make them hydrophilic. The parameters of oxygen plasma are 50 mW power, 30 s, three times.

NTA-Ni coating gold nanopillars: 2 mL of NTA-Ni solution was added to a 60x15 mm petri dish, then gold nanopillars chips were placed in this petri dish for 24-48 hours, gold nanopillars with NTA-Ni chips (AuNPs-NTA-Ni) were obtained.

Binding Pro or Hyp to AuNPs-NTA-Ni: Ethanol and H_2O were used to clean the extra NTA-Ni on the surface of AuNPs-NTA-Ni chips. 2 mL of 100 nM Pro or 100 nM Hyp neutral solution was added directly to the AuNPs-NTA-Ni solution for Raman measurements.

XPS analysis

X-ray photoelectron spectroscopy (XPS, Thermo Fisher Scientific ESCALAB 250Xi XPS, USA) was used to study the surface binding mechanism.

Raman measurements

Raman spectroscopy was performed using a Thermo Scientific DXR2xi Raman imaging microscope. The working parameters were a laser wavelength of 785 nm, an exposure time of 0.1-1 s per spectrum, a laser power of 2.5-10 mW, and a 60x water-immersion objective. Finally, Andor Solis software was used to collect the data, it collected 2000 spectra in per data at the same time. Raman data analysis was performed using MATLAB R2022a and Origin 2022b software.

Finite-element method (FEM) simulation of gold nanopillars

View Article Online
DOI: 10.1039/D5NR04125B

FEM (COMSOL Multiphysics, COMSOL Co. Ltd.) is used for numerical calculations. The optical parameters of gold and silicon are adopted from literature, respectively [26,27]. For accuracy, the finest mesh size is set to no more than 2 nm. Linearly polarized plane waves (electric field direction is parallel to the x-axis) are incident perpendicularly to the structure. Periodic boundary conditions are applied on horizontal borders. The periods along the x and y axes are set as 500 nm. The length and diameter of the nanopillar are 800 nm and 250 nm, respectively, the gold coating thickness is 50 nm, and the radius of the nanopillar cup is 100 nm.

Data pre-processed and peak assignment

Peak assignments: MATLAB was used to do peak assignments and draw SERS spectral figures. The main steps are: (1) Plot the SERS spectra of 2000 raw data; (2) Cosmic ray removed: remove the influence from Raman instrument; (3) Normalization: make all spectra have the same baseline; (4) Background removal: reduce the other purities influences; (5) Signal detection: collect all spectra with good signal; (6) Find peaks: use Pro and Hyp database to find their peaks in spectra; (7) Output figures results.

Distribution histograms of peak occurring frequency: MATLAB scripts were used to calculate the peak occurring frequency at each Raman shift. These steps are: (1) Pretreatment of multiple data; (2) Extracting effective spectra: find all spectra with rich signals; (3) Find peak frequency: summarize each peak's occurring frequency in all spectra; (4) Output Excel results, (5) Draw histograms Origin software was used to draw the distribution histograms of the SERS peaks.

Events histograms of intensity–time traces: Clampfit and Origin softwares were used for T bind and T release events histograms. The main steps are: (1) Import time trace figure to the Clampfit; (2) Event Detection; (3) Single-Chanel search; (4) Set T release as 0 and T bind as 1; (5) Run as Nonstop; (6) Export all events data in one excel file; (7) Use Origin to draw events histograms.

Deep learning classification

One-dimensional Convolutional neural network (1D-CNN) model: MATLAB was used to run the codes of the 1D-CNN model for classification and post-evaluation. A total of 6000 and 2000 peak assignment selected spectra with 1463 features were classified using 5-fold cross-validation for 1D-CNN classification model and post-evaluation model, where 80% of the spectra were used as the training set and 20% of the spectra were used as the test set. Following these steps: (1) Dataset preparation; (2) Training process; (3) Evaluation metrics.

3. Results and discussion

Sensor fabrication and measurement

For the experimental process, **Figure 1a** indicates the in-situ Raman measurements of Pro and Hyp using gold nanopillars. As conceptualized in **Figure 1b**, NTA was covalently attached to the surface of gold nanopillars by thiol bonding, then reacted with Ni^{2+} to form NTA-Ni as the specific affinity agent to capture Pro and Hyp as NTA-Ni-Pro and NTA-Ni-Hyp through chelation. The gold

View Article Online
DOI: 10.1039/D5NR04125B

nanopillar has the advantage of having a stable wide-range hot spot (**Figure 1c**) with a decay length of around 50 nm for reproducible SERS detection of large and long molecule moieties [19,20]. As the length of NTA-Ni-Pro (NTA-Ni-Hyp) is short [28], the hot spot of the gold nanopillars can cover all chains of the molecules to provide convoluted SERS spectra of both the NTA-Ni and the Pro (Hyp). The finite element method (FEM) simulation of the AuNPs with diameter of 250 nm shows wide-range hot spot at 785 nm wavelength (**Figure 1c**) when the simulated reflectance shows a localized surface plasmon resonance (LSPR) at 790 nm (**Figure S1a**). Accordingly, we fabricated AuNPs of similar diameter, the height of around 1 μm, the period of around 500 nm (**Figure 1d**). The measured reflectance shows that its LSPR dip is at 786 nm (**Figure S1b**). The fabricated AuNPs have a uniform surface and a stable structure (**Figure S2**). These results demonstrate that the fabricated AuNPs can provide reproducible SERS spectra with wide-range hot spot.

To test the binding capability of NTA to capture Pro or Hyp, we conducted in-situ Raman measurement to collect 2000 time-series SERS spectra with 0.1 s exposure time of molecules in different systems: AuNPs-NTA-Ni-Pro (**Figure 1e**), AuNPs (**Figure S3a**), and AuNPs-Pro (**Figure S3b**). The NTA-Ni was incubated on the AuNPs for 24-48 hours to form the AuNPs-NTA-Ni structure as confirmed by the XPS analysis in **Figure S4**. As a control sample of bare AuNPs, no SERS signals were observed on AuNPs themselves (**Figure S3a**). When the Pro solution was directly added to the petri dish containing the bare AuNPs chips, the water-immersion objective was dipped into it immediately for SERS measurement. Such diffusion of Pro near the AuNPs for a short time also did not show any SERS signals (**Figure S3b**). In the case of using AuNPs-NTA-Ni to bind Pro molecules, the SERS time-series spectra in **Figure 1e** shows that the unique Raman bands at 411, 618 cm^{-1} are from aromatic ring bending, and 1225 cm^{-1} as the Pro ring deformation of CH_2 and NH_2, 825 cm^{-1} for ring stretching, demonstrating the successful binding of Pro [15-16]. The 618 cm^{-1} shifts to 648 cm^{-1} due to the changes of Pro confirmation. **Figure 1f** shows the representative stochastic SERS time traces of the Pro band at 825 cm^{-1}, in which the pulses were from the binding of the AuNPs-NTA-Ni to the Pro molecules and the baseline were release of the Pro from the AuNPs-NTA-Ni. Other peaks assignments information can be found in **Table S2.** Moreover, we observed fluctuation of the SERS band position of AuNPs-NTA-Ni-Pro, such as the 825 and 1225 cm^{-1} bands in **Figure 2a** and those in **Figure S5**, which could be due to the conformation changes of the AuNPs-NTA-Ni-Pro [15].

Peak frequency analysis

Similarly, we observed stochastic and fluctuating SERS spectra of AuNPs-NTA-Ni-Hyp in **Figure 2c** and **Figure S6.** The band fluctuation is challenging for traditional analysis by SERS band intensities, because averaging band by intensity would broaden the SERS peak and decrease spectral resolution. To study the SERS band difference between the AuNPs-NTA-Ni-Pro and the AuNPs-NTA-Ni-Hyp, we used a statistical method to draw distribution histograms of the occurrence frequency for peaks assignments [29]. It can extract specific features from fluctuated SERS spectra and reduce the influence of peak intensity, demonstrating a high spectra resolution that the traditional SERS analysis cannot provide. The histograms of the occurrence frequency for all SERS spectra of AuNPs-NTA-Ni-Pro and AuNPs-NTA-Ni-Hyp were summarized in **Figure 2b** and **Figure 2d**, respectively where the peaks assignments information can be found in **Table S2.**

View Article Online
DOI: 10.1039/D5NR04125B

Figure 2b showed the longest column bar at 485 cm^{-1} due to the Pro ring vibration, and the nearest peak at 455 cm^{-1} also from same vibration mode in AuNPs-NTA-Ni-Pro. Other Pro ring bending [16] at 349, 380, 411, 618 cm^{-1}, it shows an obvious fluctuation at 380 cm^{-1} from 362 to 392 cm^{-1}, probably molecules fluctuated condition when NTA-Ni captures Pro. There is a subtle wavenumber motion of 1233 cm^{-1} to 1247 cm^{-1} due to deformation with CH_2 and NH_2 [15]. These aromatic ring modes indicate that Pro molecules entered the hot spot of AuNPs to obtain enhanced signals. Another higher column at 1290 cm^{-1} was assigned to bending of CH and NH group [16], they are the part moiety of the Pro ring. Especially, the band of nickel with oxygen [16] was obtained at 286 cm^{-1}, it demonstrated that nickel was attached to AuNPs-NTA.

In the same condition, **Figure 2d** gave Hyp information in the AuNPs-NTA-Ni-Hyp system, the longest column at 405 cm^{-1} due to Hyp ring bending. Hyp has many vibration modes that are common with Pro due to their similar molecular structure. The strong band moves from 1210 to 1245 cm^{-1} belongs to Hyp ring deformation with CH_2 and NH_2 [15], respectively. The higher column at 1288 cm^{-1} shows bending of CH and NH from ring. It is reasonable to assume a configuration of AuNPs-NTA-Ni-Hyp that Hyp bending itself close to gold nanopillar [30], Hyp has an exceptional amino acid ring with tryptophan, so they have a similar mechanism of interaction between the molecule and the gold substrate in SERS measurement. There is one band at 285 cm^{-1} associated with nickel ions and oxygen binding as Pro. Particularly, Hyp has a strong band at 1169 cm^{-1}, which is assigned to NH bending [15-16]. **Figure 2b**, **d** shows the overall change trend of the Pro / Hyp molecules in the AuNPs-NTA-Ni-Pro/Hyp system. The characteristic peak information analyzed above proves that the AuNPs-NTA-Ni system has high sensitivity in detecting Pro and Hyp.

View Article Online
DOI: 10.1039/D5NR04125B

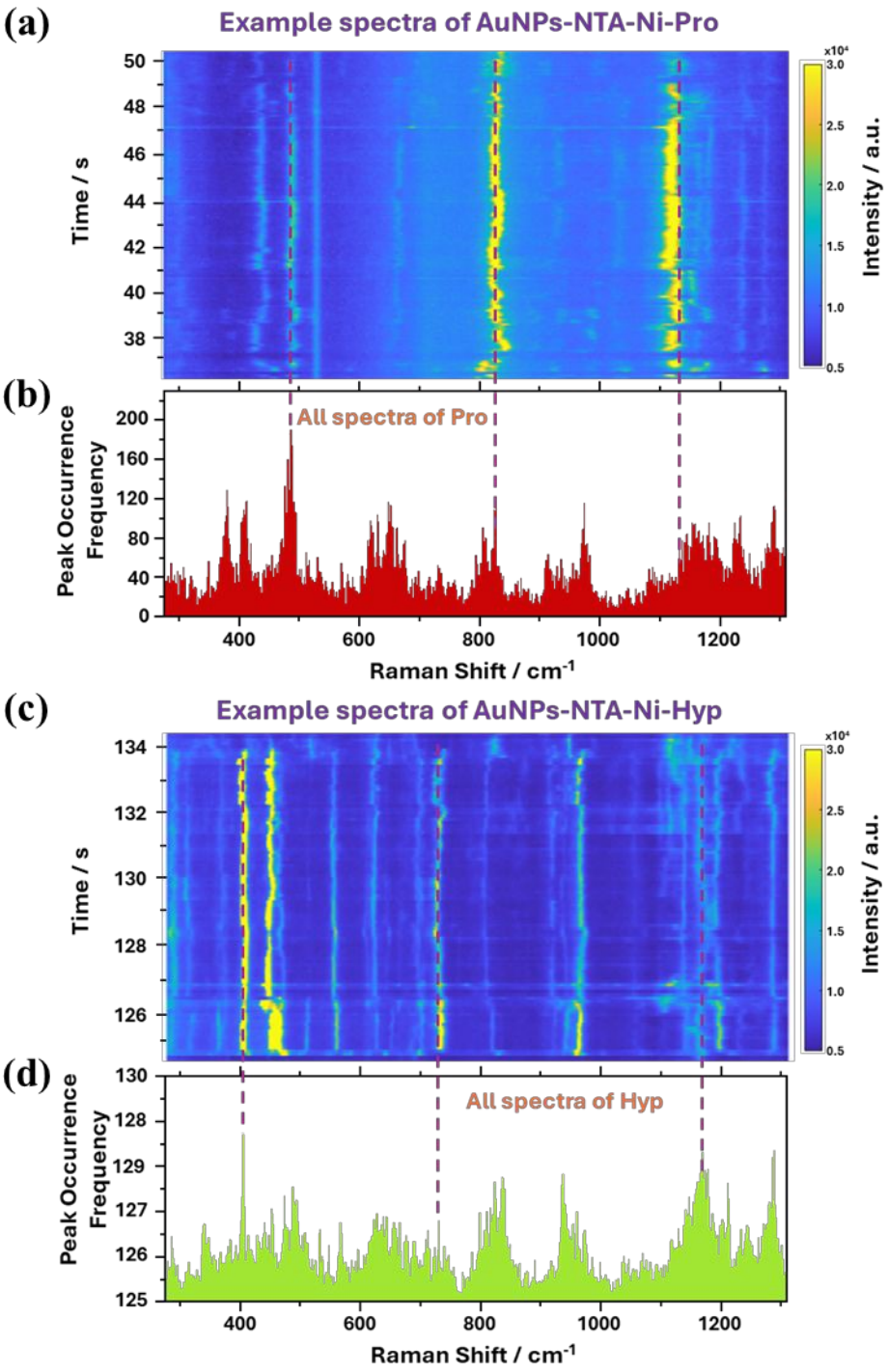

Figure 2. SERS time-series spectra of AuNPs-NTA-Ni-Pro (a) and AuNPs-NTA-Ni-Hyp (c). Distribution histograms and peaks assignments of the occurrence frequency for AuNPs-NTA-Ni-Pro (b) and AuNPs-NTA-Ni-Hyp (d) at each peak position.

Stochastic quantification of Pro and Hyp

To quantify Pro and Hyp by this method, pure Pro and Hyp at varying concentrations were firstly measured to establish linear relationships between characteristic peak frequencies and concentration.

View Article Online
DOI: 10.1039/D5NR04125B

To calculate the limitation of detection (LOD) of this method, we detected pure Pro and Hyp solutions of different concentrations to obtain the linear relationship between two characteristic peaks frequency of Pro/Hyp and concentration (**Figure S5 and S6**). Firstly, we used a series concentration of Pro and Hyp solution, with concentrations of 1 fM, 10 fM, 100 fM, 1 pM, 10 pM, 100 pM, 1 nM, 10 nM, 100 nM, and 1 μM. After obtaining their corresponding time series Raman spectra, we made distribution histograms of peak frequency. Then, we used the ratio of two characteristic peak frequencies of Pro (825, 935 cm^{-1} for ring stretching [15-16]) to the silicon frequency (520 cm^{-1}) to the concentration to obtain a good linear relationship diagram in **Figure 3a, b** with $R^2 = 0.998$ and 0.996 respectively. We fabricated gold nanopillars by coating gold layer on silicon nanopillars, so there is one silicon peak at 520 cm^{-1}. The intensity of the silicon peak was affected by (1) nanopillar uniformity, as the nanopillars coated by thin gold layer exhibited high silicon peak intensity and vice versa; and (2) intensities of SERS signals of the bond Pro/Hyp, because large amount of bond Pro/Hyp would generate strong SERS signals and baseline to overwhelm the silicon peak. By choosing the silicon peak as the internal standard, these issues of sample uniformity and bond analyte amount were all corrected.

Similarly, Hyp peaks at 405 cm^{-1} (ring bending) and 1247 cm^{-1} (ring stretching) [15-16] also exhibited strong linear correlations with concentration with R^2 =0.986 and 0.981 in **Figure 3c, d,** respectively. The calculated LODs for Pro were 0.189 pM by the 825 cm^{-1} band and 0.212 pM by the 935 cm^{-1} band, while those for Hyp were 0.434 pM for 405 cm^{-1} band and 0.576 pM for 1247 cm^{-1} band. These results show that AuNPs-NTA-Ni can obtain Pro and Hyp signals in the pM range, which has high sensitivity in quantification of biomolecules.

View Article Online
DOI: 10.1039/D5NR04125B

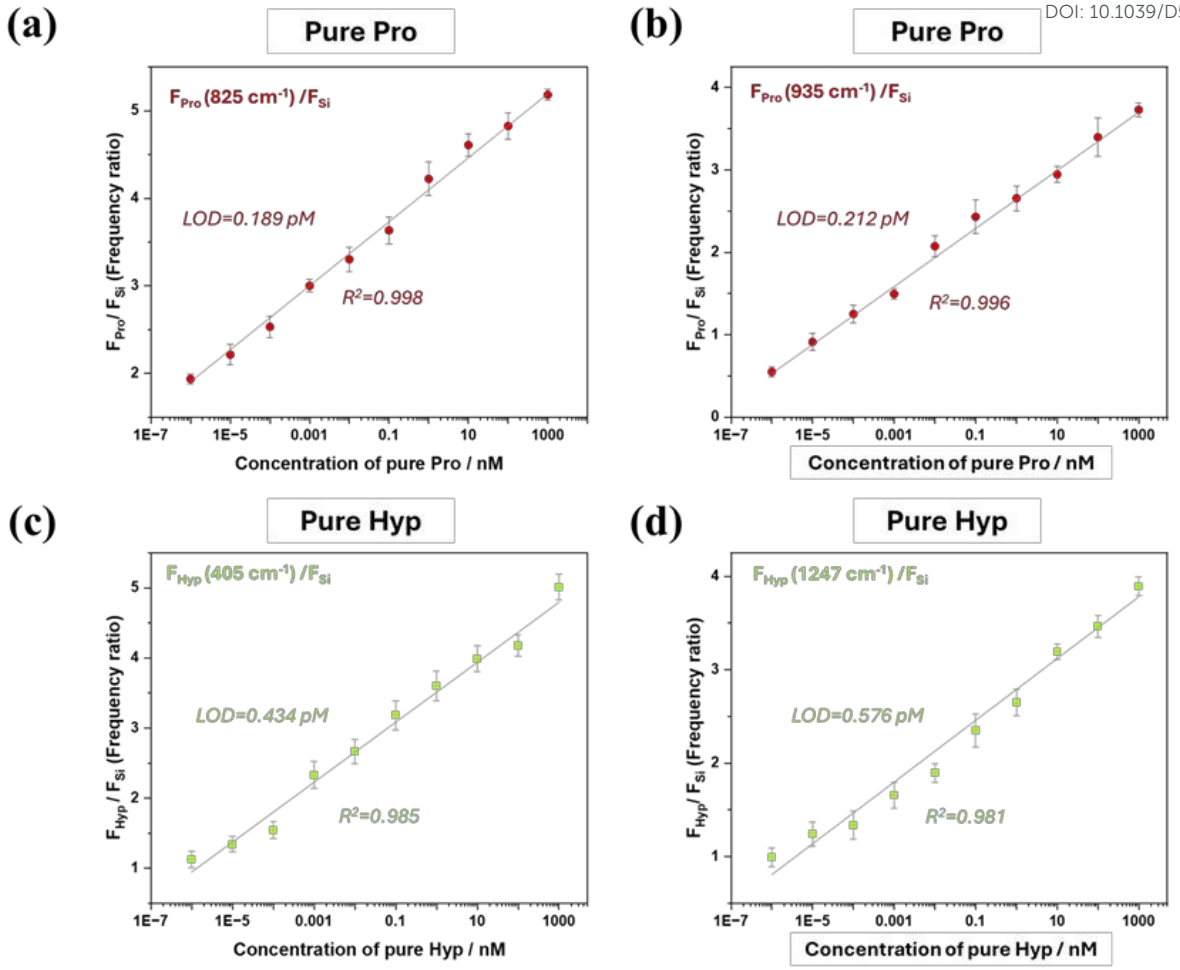

Figure 3. Stochastic quantification of pure Pro and Hyp. The linear fit of Pro and Hyp Raman peak frequency ratio of Pro 825 cm^{-1} (a), 935 cm^{-1} (b) and Hyp 405 cm^{-1} (c), 1257 cm^{-1} (d) at 1 fM to 1 μM pure Pro and Hyp concentrations. The error bars indicate the standard deviations of the peak frequency ratio for all the spectra over the detected area. Linear regression of the concentrations indicated excellent concordance between the actual and predicted results, with R^2 values of 0.998, 0.996, 0.985, 0.981 for Pro (a, b) and Hyp (c, d), respectively.

To demonstrate our method for quantification of Pro and Hyp in mixture, we tested it using mixtures of five amino acids (Pro, Hyp, Cys, His, Ser) [31-33] across six concentrations from 10 pM to 1 μM (Table 1). Following the same measurement procedure, frequencies of the characteristic peaks of Pro (825 and 935 cm^{-1}) and Hyp (405 and 1247 cm^{-1}) were normalized to those of the silicon peak at 520 cm^{-1}. The lowest concentration of Pro and Hyp in the mixture were chosen when the normalized frequencies ranged from 0.8 to 1. As shown in **Figure 4**, both exhibited excellent linear responses with R^2 = 0.992 and 0.991 for Pro and 0.988 and 0.996 for Hyp with LoDs of 0.184 nM, 0.209 nM, 0.329 nM, 0.137 nM, respectively. These findings highlight the potential of AuNPs–NTA–Ni not only for amino acid mixtures but also for detecting hydroxylated biomolecules such as HIF-1α proteins [34-36].

Table 1. The concentrations of Pro, Hyp and other amino acids in mixture.

Mixture No.	Pro	Hyp	Cys	His	Ser
1	10 pM	10 pM	10 pM	10 pM	10 pM

View Article Online
DOI: 10.1039/D5NR04125B

2	100 pM	100 pM	100 pM	100 pM	100 pM
3	1 nM	1 nM	1 nM	1 nM	1 nM
4	10 nM	10 nM	10 nM	10 nM	10 nM
5	100 nM	100 nM	100 nM	100 nM	100 nM
6	1 μM	1 μM	1 μM	1 μM	1 μM

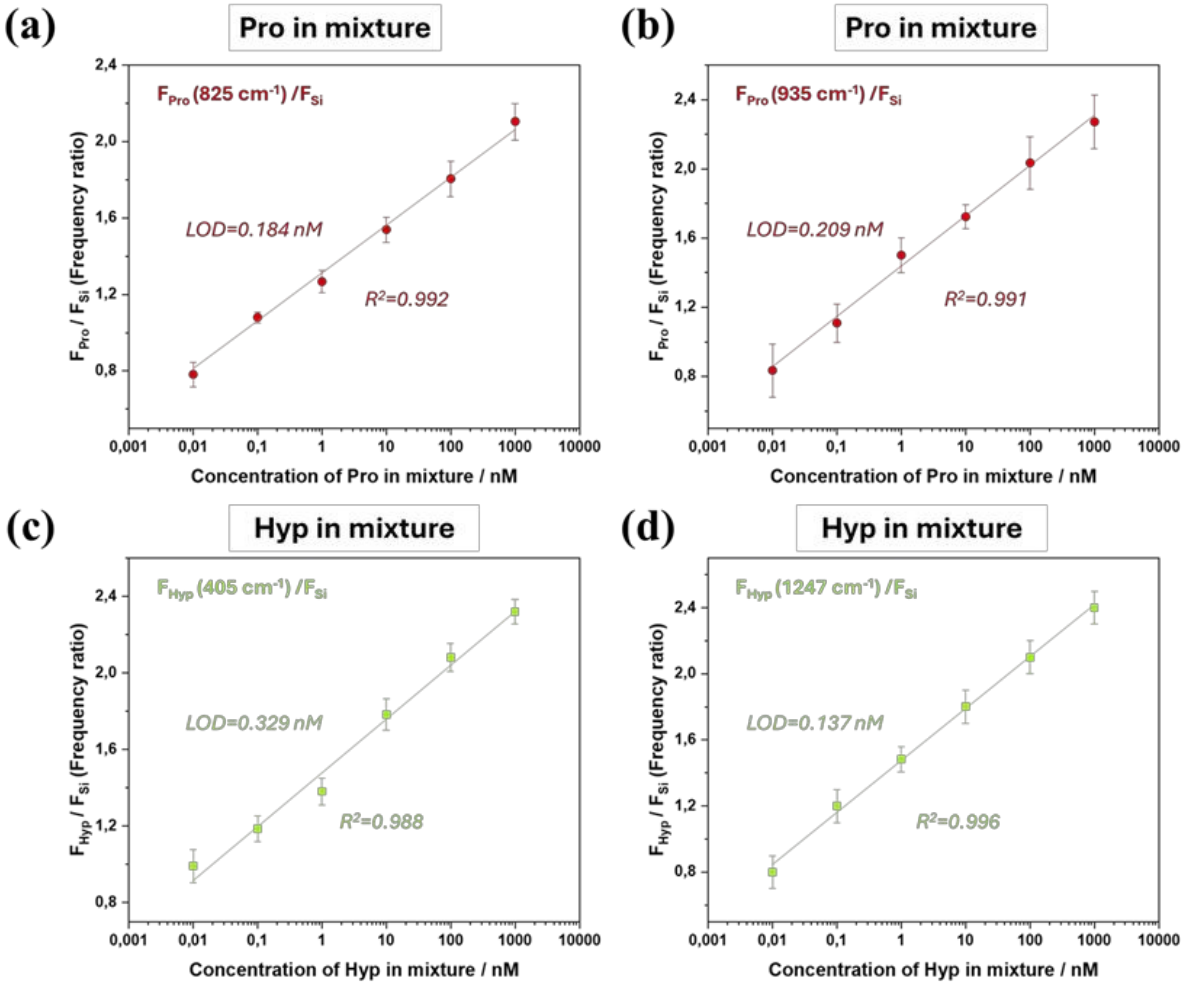

Figure 4. Stochastic quantification of Pro and Hyp in mixture. The linear fit of Pro and Hyp Raman peak frequency ratio of Pro 825 cm^{-1} (a), 935 cm^{-1} (b) and Hyp 405 cm^{-1} (c), 1257 cm^{-1} (d) at 10 pM to 1 μM pure Pro and Hyp concentrations. The error bars indicate the standard deviations of the peak frequency ratio for all the spectra over the detected area. Linear regression of the concentrations indicated excellent concordance between the actual and predicted results, with R^2 values of 0.992, 0.991, 0.988, 0.996 for Pro (a, b) and Hyp (c, d), respectively.

Stochastic binding kinetics

The LoDs of Pro and Hyp in mixture are almost 3 order lower than those in pure solution, which highlighted the competitive chelation binding of the AuNPs-NTA-Ni to the Pro/Hyp by other amino acids in the mixture. To study the competitive binding, we calculated the time constants of association (k_{on}) and dissociation (k_{off}) with SERS time traces with intensity changes [22]. As shown in **Figure 5a,**

View Article Online
DOI: 10.1039/D5NR04125B

b, the time traces of Raman intensity of SERS peak at 825 cm^{-1} for Pro and 405 cm^{-1} for Hyp were extracted from the corresponding SERS time series of specific concentrations in **Figure S5 and S6**. The duration of the transient binding event corresponds to high Raman intensity with the binding time (T-bind), i.e., the time the Pro/Hyp remains bound to the AuNPs-NTA-Ni. Conversely, the duration of the low-Raman-intensity event represents the interval between two consecutive binding events (T-release). Similar traces were also observed for pure Hyp and Pro in different concentrations (**Figure S7 and S8**).

Figure 5c, d show examples of the extracted histogram distributions of the T-bind and T-release are well described by single-exponential statistics to exp(t/T), where *T* is the characteristic time constant, indicating stochastic first-order association/dissociation dynamics at the dominant hotspot receptor. Histograms of different concentrations are in **Figure S9 and S10**. The reciprocal of the characteristic binding time $1/\langle T_{bind}\rangle$ increases linearly with analyte concentration [P]: $1/\langle T_{bind}\rangle = k_{on}[P]$ in **Figure 5e**, yielding the associate rate constant k_{on}. Then, the dissociation frequency $1/\langle T_{release}\rangle$ is essentially concentration-independent (**Figure 5f**), yielding the dissociation rates constant $k_{off} = 1/\langle T_{release}\rangle$. From the slopes and plateaus, we extracted $k_{on,\ pure\ Pro} = (4.20 \pm 0.5)\ x10^4\ M^{-1}\ s^{-1}$ and $k_{on,\ pure\ Hyp} = (4.63 \pm 0.5)\ x10^4\ M^{-1}\ s^{-1}$, while the $k_{off,\ pure\ Pro} = 0.22 \pm 0.05\ s^{-1}$ and $k_{off,\ pure\ Hyp} = 0.26 \pm 0.07\ s^{-1}$. Similarly in **Figure 5g, h**, the Pro and Hyp in mixture demonstrated concentration-dependent $k_{on,\ mix\ Pro} = (7.60 \pm 0.9)\ M^{-1}\ s^{-1}$ and $k_{on,\ mix\ Hyp} = (7.08 \pm 0.8)\ M^{-1}\ s^{-1}$ and the concentration-independent $k_{off,\ mix\ Pro} = 0.25 \pm 0.06\ s^{-1}$ and $k_{off,\ mix\ Hyp} = 0.24 \pm 0.08\ s^{-1}$.

These results confirm the reversible bimolecular interaction between the amino acids and the NTA receptor on the gold nanopillar with similar probabilities: e.g. NTA-Ni + Hyp ⇌ NTA-Ni • Hyp in both pure solution and mixture. It is reasonable to assume that the binding kinetics of Pro and Hyp were similar due to the tiny difference in their molecular structures by the small hydroxyl group. Meanwhile, the competing binding from other amino acids decreased the associate rate constants of Pro and Hyp in mixture ($k_{on,\ mix\ Hyp}$ and $k_{on,\ mix\ Pro}$) by almost 4 orders against those in pure solution ($k_{on,\ pure\ Hyp}$ and $k_{on,\ pure\ Pro}$). This contributed to the 3-order difference between the LoDs of the AnNP-NTA-Ni sensors in pure solution and mixture.

Moreover, the higher $k_{on,\ mix\ Pro} = (7.60 \pm 0.9)\ M^{-1}\ s^{-1}$ than the $k_{on,\ mix\ Hyp} = (7.08 \pm 0.8)\ M^{-1}\ s^{-1}$ meant higher binding probability of Pro than that of Hyp to the AuNP-NTA-Ni in the mixture. This led to lower average LoD of Pro in mixture as 0.20 nM by the 825 and 935 cm^{-1} peaks (**Figure 4a, b**) than that of Hyp in mixture as 0.23 nM by the 405 and 1247 cm^{-1} peaks (**Figure 4c, d**). However, the LoD of Hyp in mixture (0.137 nM) calculated by the 1247 cm^{-1} peaks did not follow this trend, which might be due to the Hyp conformation change and resultant fluctuating SERS bands. This suggests that the SERS band fluctuation affected the LoD significantly and the LoD calculation using single SERS band is not reliable.

View Article Online
DOI: 10.1039/D5NR04125B

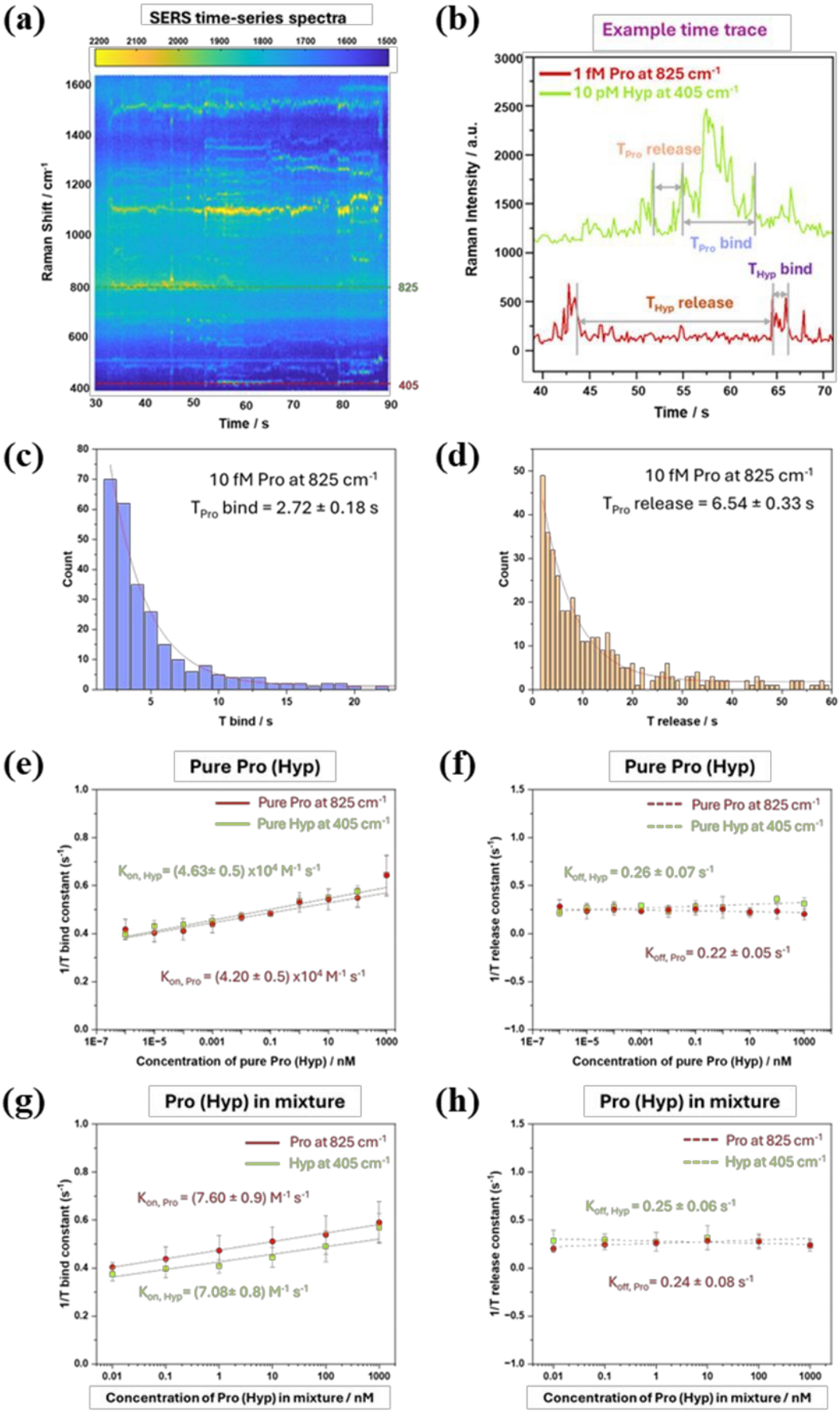

View Article Online
DOI: 10.1039/D5NR04125B

Figure 5. Binding kinetics of Pro, Hyp and mixture on NTA-modified gold nanopillars. (a) SERS time-series spectra of Pro/Hyp in mixture. (b) Representative Raman time traces of Pro and Hyp show transient binding and releasing events. (c, d) Event histogram examples of intensity–time traces. T_bind represents the binding duration, while T_release is the interval between two consecutive binding events. Solid lines indicate single-exponential fits, providing the characteristic time constants T-bind and T-release. (e-h) Association frequency ($1/\langle T_{bind} \rangle$) and dissociation frequency ($1/\langle T_{release} \rangle$) as functions of Pro, Hyp (e, f) and mixture (g, h) at their varying concentrations. The solid lines show linear fits used to extract the association rate, whereas the dotted lines represent constant fits used to determine the dissociation rate.

Deep learning identification

The SERS band fluctuation of the AuNPs-NTA-Ni-Pro and the AuNPs-NTA-Ni-Hyp necessitated the use of deep learning models for data analysis and identification. Accordingly, we developed a one-dimensional convolutional neural network (1D-CNN) model for the spectra classification of AuNPs-NTA-Ni-Pro and AuNPs-NTA-Ni-Hyp in **Figure 6a**. 6000 spectra of the AuNPs-NTA-Ni-Pro and the AuNPs-NTA-Ni-Hyp, respectively, were divided as 4800 spectra for model training and 1200 ones for testing. **Figure S11a** shows the low loss curve and the high accuracy curve of the training model with increasing training epochs, which means the great classification performance of the trained 1D-CNN model for identifying the AuNPs-NTA-Ni-Pro and AuNPs-NTA-Ni-Hyp spectra. For the training 4800 spectra data of AuNPs-NTA-Ni-Pro and AuNPs-NTA-Ni-Hyp, the classification accuracies are 99.5 % for Pro and 99.1 % for Hyp, as presented in **Figure S11b**. While at the testing step of 1200 spectra, the classification accuracies for the Pro and Hyp were 96.5% for Hyp and 95.9 % for Pro in **Figure 6b**.

The CNN operates on individual single-shot spectra, each of which corresponds to one time point within the 2000-frame SERS time series (0.1 s per frame). Spectra are not averaged, not grouped by time, and no time index is provided to the model. Low-signal spectra are removed through preprocessing and peak assignment, and all remaining spectra are treated as independent samples for classification. To test the practical use of the trained 1D-CNN model, another set of 2000 completely new and independently prepared spectra—acquired on fresh Au nanopillar substrates, on a different measurement day, and using newly prepared NTA–Ni and Pro/Hyp solutions—were fed into the network in a predict-only mode for external post-evaluation analysis. As exhibited in **Figure 6c**, classification accuracy of 89.6 % for Hyp and 86.9% for Pro are obtained in the confusion matrix of post-evaluation analysis, demonstrating the significant performance of the trained 1D-CNN model to differentiate new SERS spectra of AuNPs-NTA-Ni-Pro and AuNPs-NTA-Ni-Hyp. The receiver operating characteristics (ROC) in **Figure 6d.** It shows both high sensitivity and high specificity of the model in identifying new spectra of Pro and Hyp.

View Article Online
DOI: 10.1039/D5NR04125B

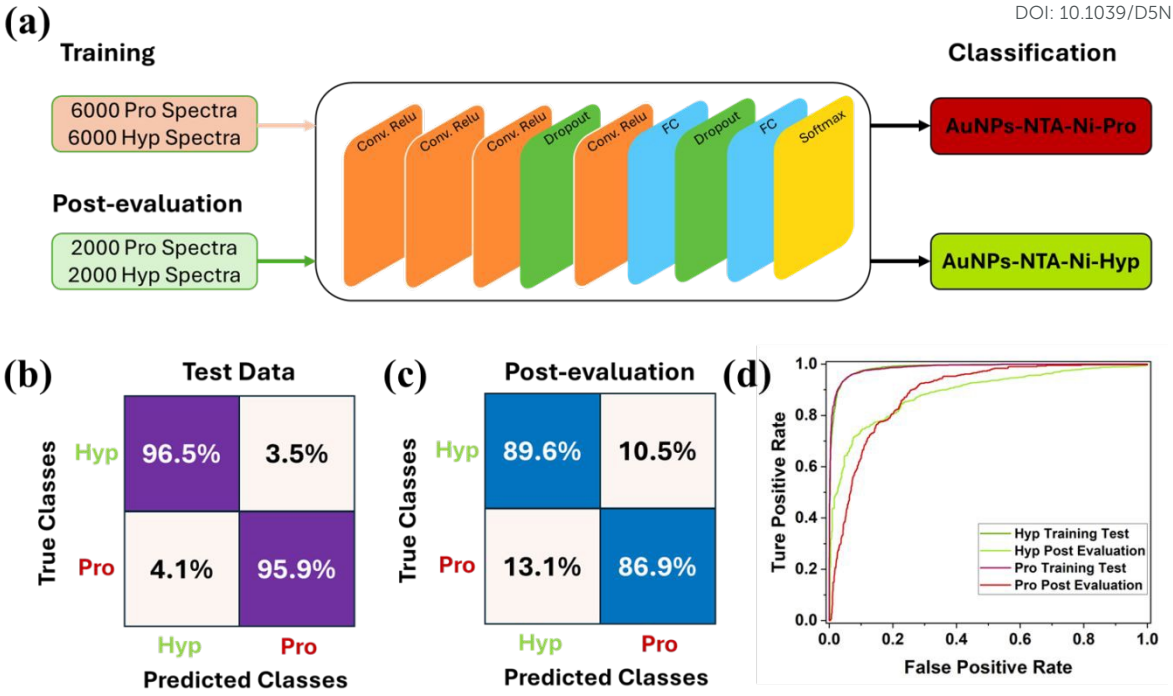

Figure 6. Deep learning process for identification of AuNPs-NTA-Ni-Pro and AuNPs-NTA-Ni-Hyp by a 1D-CNN model. (a) The architecture of the 1D-CNN model. (b) The testing classification accuracy of 96.5% for Hyp and 95.9% for Pro. (c) The post-evaluation classification accuracy of 89.6% for Hyp and 86.9% for Pro. (d) The ROC figure of Hyp and Pro.

4. Conclusion

In summary, the stochastic sensing platform based on AuNPs-NTA-Ni was designed and used to reversibly capture and detect Pro and Hyp by SERS. The distribution histograms of occurrence frequency provided the band features between Pro and Hyp, which can be used to achieve fast quantitative analysis within 30 min. Accordingly, we got good LoDs in mixture as between 0.184 nM and 0.209 nM for Pro and between 0.137 nM and 0.329 nM for Hyp, respectively. The transient signals of different bands extracted from the time-series SERS spectra were analyzed for the binding kinetics of AuNPs-NTA-Ni to Pro/Hyp. The competing binding in mixture from other amino acids decreased the associate rate constants of Pro and Hyp by almost 4 orders against those in pure solution, which contributed to the 3-order difference between the LoDs of the AnNP-NTA-Ni sensors in pure solution and mixture. To overcome the uncertainty of LoD calculation by the fluctuating SERS bands, we used the deep learning identification by a 1D-CNN model: the test results of Pro and Hyp are 95.9% and 96.5%, the post-evaluation results of new data are 86.9% and 89.9%, respectively. Our work demonstrated a new SERS sensing method based on reversible binding and deep learning analysis, setting a base for the challenging hydroxylation detection in, for example, rapid diagnosis for biomarkers of cancer diseases.

Authors Contributions

View Article Online
DOI: 10.1039/D5NR04125B

Yuan Zhang fabricated the gold nanopillars chips, determined the Raman measurement protocol, collected Raman spectra, analyzed the Raman spectra, and wrote the manuscript. Kuo Zhan wrote the scripts for Raman data preprocessing, peak occurrence frequency calculation and developed a 1D-CNN model for Pro/Hyp discrimination. Peilin Xin contributed to writing the Raman spectra preprocessing, data selection scripts and revised the manuscript. Yingqi Zhao contributed to the Raman measurement suggestion and revised the manuscript. Ibrar Alam helped to draw time trace histograms and revised the manuscript. Shubo Wang provided UV-Vis measurement devices and revised the manuscript. Kai Liu did the simulation and revised the manuscript. Aliaksandr Hubarevich contributed to the gold nanopillars simulation. Xuejin Zhang supervised the simulation. Jianan Huang conceived the idea, acquired funding, supervised the work, and revised the manuscript. The manuscript was written with contributions from all authors. All authors have approved the final version of the manuscript.

Conflicts of interest

There are no conflicts to declare.

Data availability

The authors declare that the data supporting the findings of this study are available within the paper and its SI files. Data is also available from the corresponding author upon reasonable request.

Supplementary information is available.

The codes for data analysis and all raw SERS data are in Github. The website link:

KuoZHAN/Surface-enhanced-Raman-spectroscopic-detection-of-proline-and-hydroxylated-proline-: CNN and post-evaluation model with raw data

Acknowledgements

This research receives support from Biocenter Oulu emerging project (DigiRaman), spearhead project 2024 - 2027 and DigiHealth project (No. 326291), a strategic profiling project at the University of Oulu that is supported by the Academy of Finland and the University of Oulu. Yuan Zhang acknowledges the China Scholarship Council for a scholarship for doctoral study at the University of Oulu. The authors thank Professor Xia Yang (Southwest University, China) for valuable discussion about NTA binding

View Article Online
DOI: 10.1039/D5NR04125B

References

(1) Szabados, L.; Savouré, A. Proline: A Multifunctional Amino Acid. *Trends Plant Sci* **2010**, *15* (2), 89–97. https://doi.org/10.1016/j.tplants.2009.11.009.

(2) Semenza, G. L. Regulation of Mammalian O $_2$ Homeostasis by Hypoxia-Inducible Factor 1. *Annu Rev Cell Dev Biol* **1999**, *15* (1), 551–578. https://doi.org/10.1146/annurev.cellbio.15.1.551.

(3) Maxwell, P. H.; Wiesener, M. S.; Chang, G.-W.; Clifford, S. C.; Vaux, E. C.; Cockman, M. E.; Wykoff, C. C.; Pugh, C. W.; Maher, E. R.; Ratcliffe, P. J. The Tumour Suppressor Protein VHL Targets Hypoxia-Inducible Factors for Oxygen-Dependent Proteolysis. *Nature* **1999**, *399* (6733), 271–275. https://doi.org/10.1038/20459.

(4) Bruick, R. K.; McKnight, S. L. A Conserved Family of Prolyl-4-Hydroxylases That Modify HIF. *Science (1979)* **2001**, *294* (5545), 1337–1340. https://doi.org/10.1126/science.1066373.

(5) Epstein, A. C. R.; Gleadle, J. M.; McNeill, L. A.; Hewitson, K. S.; O'Rourke, J.; Mole, D. R.; Mukherji, M.; Metzen, E.; Wilson, M. I.; Dhanda, A.; Tian, Y.-M.; Masson, N.; Hamilton, D. L.; Jaakkola, P.; Barstead, R.; Hodgkin, J.; Maxwell, P. H.; Pugh, C. W.; Schofield, C. J.; Ratcliffe, P. J. C. Elegans EGL-9 and Mammalian Homologs Define a Family of Dioxygenases That Regulate HIF by Prolyl Hydroxylation. *Cell* **2001**, *107* (1), 43–54. https://doi.org/10.1016/S0092-8674(01)00507-4.

(6) Ivan, M.; Kondo, K.; Yang, H.; Kim, W.; Valiando, J.; Ohh, M.; Salic, A.; Asara, J. M.; Lane, W. S.; Kaelin Jr., W. G. HIFα Targeted for VHL-Mediated Destruction by Proline Hydroxylation: Implications for O $_2$ Sensing. *Science (1979)* **2001**, *292* (5516), 464–468. https://doi.org/10.1126/science.1059817.

(7) Jaakkola, P.; Mole, D. R.; Tian, Y.-M.; Wilson, M. I.; Gielbert, J.; Gaskell, S. J.; Kriegsheim, A. von; Hebestreit, H. F.; Mukherji, M.; Schofield, C. J.; Maxwell, P. H.; Pugh, ‡ Christopher W.; Ratcliffe, ‡ Peter J. Targeting of HIF-α to the von Hippel-Lindau Ubiquitylation Complex by O $_2$ -Regulated Prolyl Hydroxylation. *Science (1979)* **2001**, *292* (5516), 468–472. https://doi.org/10.1126/science.1059796.

(8) Zhou, T.; Erber, L.; Liu, B.; Gao, Y.; Ruan, H.-B.; Chen, Y. Proteomic Analysis Reveals Diverse Proline Hydroxylation-Mediated Oxygen-Sensing Cellular Pathways in Cancer Cells. *Oncotarget* **2016**, *7* (48), 79154–79169. https://doi.org/10.18632/oncotarget.12632.

(9) J., R. Methods for Measuring Hydroxyproline and Estimating In Vivo Rates of Collagen Synthesis and Degradation. In *Fibrosis Research*; Humana Press: Totowa, NJ, 2005; pp 189–207. https://doi.org/10.1385/1-59259-940-0:189.

(10) Kumar Srivastava, A.; Khare, P.; Kumar Nagar, H.; Raghuwanshi, N.; Srivastava, R. Hydroxyproline: A Potential Biochemical Marker and Its Role in the Pathogenesis of

View Article Online
DOI: 10.1039/D5NR04125B

Different Diseases. *Curr Protein Pept Sci* **2016**, *17* (6), 596–602. https://doi.org/10.2174/1389203717666151201192247.

(11) Ábrahám, E.; Hourton-Cabassa, C.; Erdei, L.; Szabados, L. Methods for Determination of Proline in Plants. In *Methods in Molecular Biology*; 2010; Vol. 639, pp 317–331. https://doi.org/10.1007/978-1-60761-702-0_20.

(12) Shen, T.; Zhang, C.; Liu, F.; Wang, W.; Lu, Y.; Chen, R.; He, Y. High-Throughput Screening of Free Proline Content in Rice Leaf under Cadmium Stress Using Hyperspectral Imaging with Chemometrics. *Sensors* **2020**, *20* (11), 3229. https://doi.org/10.3390/s20113229.

(13) Cotte, J. F.; Casabianca, H.; Giroud, B.; Albert, M.; Lheritier, J.; Grenier-Loustalot, M. F. Characterization of Honey Amino Acid Profiles Using High-Pressure Liquid Chromatography to Control Authenticity. *Anal Bioanal Chem* **2004**, *378* (5), 1342–1350. https://doi.org/10.1007/s00216-003-2430-z.

(14) Chan, S. W. P.; Greaves, J.; Da Silva, N. A.; Wang, S.-W. Assaying Proline Hydroxylation in Recombinant Collagen Variants by Liquid Chromatography-Mass Spectrometry. *BMC Biotechnol* **2012**, *12* (1), 51. https://doi.org/10.1186/1472-6750-12-51.

(15) Cárcamo, J. J.; Aliaga, A. E.; Clavijo, E.; Garrido, C.; Gómez-Jeria, J. S.; Campos-Vallette, M. M. Proline and Hydroxyproline Deposited on Silver Nanoparticles. A Raman, SERS and Theoretical Study. *Journal of Raman Spectroscopy* **2012**, *43* (6), 750–755. https://doi.org/10.1002/jrs.3092.

(16) Guerrero, A. R.; Aroca, R. F. Surface-enhanced Raman Scattering of Hydroxyproline. *Journal of Raman Spectroscopy* **2012**, *43* (4), 478–481. https://doi.org/10.1002/jrs.3065.

(17) Zhao, Y.; Zhan, K.; Xin, P.-L.; Chen, Z.; Li, S.; De Angelis, F.; Huang, J.-A. Single-Molecule SERS Discrimination of Proline from Hydroxyproline Assisted by a Deep Learning Model. *Nano Lett* **2025**, *25* (18), 7499–7506. https://doi.org/10.1021/acs.nanolett.5c01177.

(18) Yang, Z.; Chen, G.; Shen, J.; Ma, C.; Gu, J.; Zhu, C.; Li, L.; Gao, H. A Hydrogen Bonding Based SERS Method for Direct Label-Free L-Hydroxyproline Detection. *Spectrochim Acta A Mol Biomol Spectrosc* **2023**, *299*, 122834. https://doi.org/10.1016/j.saa.2023.122834.

(19) Huang, J.-A.; Zhao, Y.-Q.; Zhang, X.-J.; He, L.-F.; Wong, T.-L.; Chui, Y.-S.; Zhang, W.-J.; Lee, S.-T. Ordered Ag/Si Nanowires Array: Wide-Range Surface-Enhanced Raman Spectroscopy for Reproducible Biomolecule Detection. *Nano Lett* **2013**, *13* (11), 5039–5045. https://doi.org/10.1021/nl401920u.

(20) Zhao, Y.; Huang, J.-A.; Zhang, Z.; Chen, X.; Zhang, W. Quantitative Analysis of Multiplex-Components and Double Stranded DNA by Wide-Range Surface-

Enhanced Raman Spectroscopy Based on Ordered Ag/Si Nanowire Arrays. *J Mater Chem A Mater* **2014**, *2* (26), 10218–10224. https://doi.org/10.1039/c4ta00904e.

(21) Wang, K.; Zhang, S.; Zhou, X.; Yang, X.; Li, X.; Wang, Y.; Fan, P.; Xiao, Y.; Sun, W.; Zhang, P.; Li, W.; Huang, S. Unambiguous Discrimination of All 20 Proteinogenic Amino Acids and Their Modifications by Nanopore. *Nat Methods* **2024**, *21* (1), 92–101. https://doi.org/10.1038/s41592-023-02021-8.

(22) Wei, R.; Gatterdam, V.; Wieneke, R.; Tampé, R.; Rant, U. Stochastic Sensing of Proteins with Receptor-Modified Solid-State Nanopores. *Nat Nanotechnol* **2012**, *7* (4), 257–263. https://doi.org/10.1038/nnano.2012.24.

(23) Li, P.; Zhou, B.; Ge, M.; Jing, X.; Yang, L. Metal Coordination Induced SERS Nanoprobe for Sensitive and Selective Detection of Histamine in Serum. *Talanta* **2022**, *237*, 122913. https://doi.org/10.1016/j.talanta.2021.122913.

(24) Kaya, M.; Volkan, M. New Approach for the Surface Enhanced Resonance Raman Scattering (SERRS) Detection of Dopamine at Picomolar (PM) Levels in the Presence of Ascorbic Acid. *Anal Chem* **2012**, *84* (18), 7729–7735. https://doi.org/10.1021/ac3010428.

(25) Cao, X.; Qin, M.; Li, P.; Zhou, B.; Tang, X.; Ge, M.; Yang, L.; Liu, J. Probing Catecholamine Neurotransmitters Based on Iron-Coordination Surface-Enhanced Resonance Raman Spectroscopy Label. *Sens Actuators B Chem* **2018**, *268*, 350–358. https://doi.org/10.1016/j.snb.2018.04.117.

(26) Johnson, P. B.; Christy, R. W. Optical Constants of the Noble Metals. *Phys Rev B* **1972**, *6* (12), 4370–4379. https://doi.org/10.1103/PhysRevB.6.4370.

(27) Schinke, C.; Peest, P. C.; Bothe, K.; Schmidt, J.; Brendel, R.; Vogt, M. R.; Kröger, I.; Winter, S.; Schirmacher, A.; Lim, S.; Nguyen, H. T.; Macdonald, D. Experimental Determination of the Uncertainty of the Absorption Coefficient of Crystalline Silicon. *Energy Procedia* **2015**, *77*, 170–178. https://doi.org/10.1016/j.egypro.2015.07.025.

(28) Wang, X.; Liu, Q.; Tan, X.; Liu, L.; Zhou, F. Covalent Affixation of Histidine-Tagged Proteins Tethered onto Ni-Nitrilotriacetic Acid Sensors for Enhanced Surface Plasmon Resonance Detection of Small Molecule Drugs and Kinetic Studies of Antibody/Antigen Interactions. *Analyst* **2019**, *144* (2), 587–593. https://doi.org/10.1039/C8AN01794H.

(29) Li, W.; Guo, L.; Ding, X.-L.; Ding, Y.; Ji, L.-N.; Xia, X.-H.; Wang, K. High-Throughput Single-Molecule Surface-Enhanced Raman Spectroscopic Profiling of Single-Amino Acid Substitutions in Peptides by a Gold Plasmonic Nanopore. *ACS Nano* **2024**, *18* (29), 19200–19207. https://doi.org/10.1021/acsnano.4c04775.

(30) Hernández, B.; Tinacci, L.; Coïc, Y.-M.; Chenal, A.; Cohen, R.; Sanchez-Cortes, S.; Ghomi, M. Tryptophan Tight Binding to Gold Nanoparticles Induces Drastic Changes

in Indole Ring Raman Markers. *The Journal of Physical Chemistry C* **2018**, *122*(24), 13034–13046. https://doi.org/10.1021/acs.jpcc.8b02261.

View Article Online
DOI: 10.1039/D5NR04125B

(31) Li, X., et al. "Gold Nanoparticle-Decorated MOF for Ultrasensitive SERS Detection of Cysteine in Live Cells." *Analytical Chemistry*, vol. 95, no. 15, 2023, pp. 6231-39.

(32) Kumar, A., and S. Kim. "Plasmonic Paper-Based SERS Sensor for Visual Detection of Histidine Using ZIF-8 Encapsulated Silver Nanoparticles." *Microchimica Acta*, vol. 191, no. 3, 2024, p. 128.

(33) Yang, L., et al. "Molecularly Imprinted Polymer-Based SERS Sensor for the Specific Recognition of Serine." *ACS Applied Materials & Interfaces*, vol. 15, no. 20, 2023, pp. 24548-57.

(34) Wang, Y., Chen, L., & Liu, Z. (2023). A plasmonic immunosensor for ultrasensitive detection of HIF-1α in tumor biopsies. *Analytical Chemistry*, *95*(15), 6231–6239. https://doi.org/10.1021/acs.analchem.3c00567.

(35) Zhang, K., Xu, M., & Li, H. (2024). CRISPR-Cas12a-driven electrochemical biosensor for the detection of HIF-2α mRNA in renal cell carcinoma. *Biosensors and Bioelectronics*, *245*, 115801. https://doi.org/10.1016/j.bios.2023.115801.

(36) Lee, S., Park, J., & Singh, A. (2023). A SERS-based multiplexed assay for simultaneous detection of HIF-1α and VEGF in hypoxic cells. *ACS Sensors*, *8*(8), 3124–3133. https://doi.org/10.1021/acssensors.3c00812.

View Article Online
DOI: 10.1039/D5NR04125B

Data availability statements

The authors declare that the data supporting the findings of this study are available within the paper and its SI files. Data is also available from the corresponding author upon reasonable request.

The data supporting this article have been included as part of the Supplementary Information.

The codes for data analysis and all raw SERS data are in Github. The website link: KuoZHAN/Surface-enhanced-Raman-spectroscopic-detection-of-proline-and-hydroxylated-proline-: CNN and post-evaluation model with raw data